

NASA Contractor Report 2986

NASA
CR
2986
c.1

TECH LIBRARY KAFB, NM
0061623

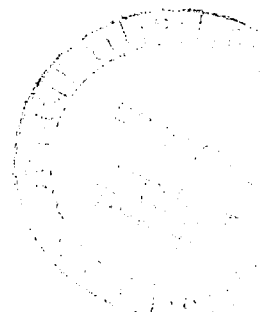
LOAN COPY RETURN
AFWL TECHNICAL LIB
KIRTLAND AFB, NM

Transitional Boundary-Layer Solutions Using a Mixing-Length and a Two-Equation Turbulence Model

E. Clay Anderson and David C. Wilcox

CONTRACT NAS1-14517
APRIL 1978

NASA





NASA Contractor Report 2986

Transitional Boundary-Layer Solutions Using a Mixing-Length and a Two-Equation Turbulence Model

E. Clay Anderson and David C. Wilcox
DCW Industries, Inc.
Studio City, California

Prepared for
Langley Research Center
under Contract NAS1-14517



National Aeronautics
and Space Administration

**Scientific and Technical
Information Office**

1978

SUMMARY

Boundary-layer solutions have been obtained using the conventional two-layer mixing-length turbulence model and the Wilcox-Traci two-equation model of turbulence. Both flat-plate and blunt-body geometries have been considered. The most significant result of the study is development of approximations for the two-equation model which permit streamwise stepsize comparable to that used in mixing-length computations. Prior to this study, calculations with the two-equation model could be made only by using stepsizes an order of magnitude smaller than those used in corresponding mixing-length computations. Additionally, a set of model-equation boundary conditions have been devised which apply equally well to both flat-plate and blunt-body geometries. Solutions obtained with the two-equation turbulence model are compared with experimental data and/or corresponding solutions obtained using the mixing-length model. Agreement is satisfactory for flat-plate boundary layers. For blunt bodies, results indicate that further investigation is necessary.

CONTENTS

SECTION		PAGE
	LIST OF SYMBOLS.....	vii
1	INTRODUCTION.....	1
2	ANALYSIS.....	2
	2.1 Governing Equations.....	3
	2.1.1 Boundary Conditions for the Governing Equations.....	7
	2.1.2 Fluid Properties at the Boundary-Layer Edge.....	8
	2.2 Mixing-Length Turbulence Model.....	10
	2.2.1 Inner-Eddy-Viscosity Approximation..	11
	2.2.2 Outer-Eddy-Viscosity Approximation..	11
	2.3 Two-Equation Turbulence Model.....	12
	2.3.1 Model-Equation Boundary Conditions..	14
	2.3.2 Modified Forms of the Model Equations.....	18
	2.3.3 Description of the Numerical Method and Essential Features of the Computer Code.....	21
3	RESULTS AND DISCUSSION.....	23
	3.1 Flat-Plate Boundary-Layer Calculations.....	24
	3.2 Blunt-Body Boundary-Layer Calculations.....	33
4	CONCLUDING REMARKS.....	39
	REFERENCES.....	40

LIST OF SYMBOLS

SYMBOL	DEFINITION
A^+	Damping factor in mixing-length turbulence model
a^*	Reference length
C	Density-viscosity product, $\bar{\rho} \bar{\mu}$
\bar{c}	Constant in Sutherland's law
C_f	Skin-friction coefficient
c_p	Specific heat at constant pressure
D	Diffusion coefficient in model equations
e	Turbulent mixing energy
H	Enthalpy
\bar{H}	Normalized enthalpy, H/H_e
k	Roughness height
k^+	Roughness height Reynolds number, $\rho_w u_{\tau} k / (\mu_w \sigma^2)$
ℓ	Scaled turbulent mixing length
$\tilde{\ell}$	Turbulent length scale
M	Mach number
N_{Pr}	Prandtl number
$N_{Pr,T}$	Turbulent Prandtl number
N_{Re}	Reynolds number
N_{St}	Stanton number
P	Pressure
Q	Heating rate

LIST OF SYMBOLS (Cont)

SYMBOL	DEFINITION
r	Body radius measured from axis or plane of symmetry
r_s	Shock radius measured from axis or plane of symmetry
$S_B(v_w^+)$	Universal function of surface mass-injection
$S_R(k^+)$	Universal function of surface roughness
T	Temperature
\tilde{T}_i	Turbulent intensity
u	Tangential velocity
u_s	Velocity tangent to shock
u_τ	Friction velocity
\bar{u}	Normalized tangential velocity, u/u_e
V	Transformed normal velocity
v	Scaled normal velocity
v_s	Velocity normal to shock
v'	Flutuating component of normal velocity
v_w^+	Stress scaled normal velocity at surface
w	Turbulent dissipation rate
x	Coordinate along body surface
y	Scaled coordinate normal to surface
\tilde{y}	Coordinate normal to surface
y^+	Stress scaled coordinate normal to surface
z	Body coordinate along plane or axis of symmetry

LIST OF SYMBOLS (Cont)

SYMBOL	DEFINITION
z_s	Shock coordinate along plane or axis of symmetry
α_1, α_2	Parameters in turbulence model equations
β	Pressure gradient parameter
β_1, β_2	Parameters in turbulence model equations
γ	Specific heat ratio
γ_e	Effective specific heat ratio
$\gamma_{i,\eta}$	Normal intermittency factor
δ	Boundary-layer thickness
δ_c	Compressible displacement thickness
δ_k	Incompressible displacement thickness
ϵ^+	Normalized eddy viscosity, μ_T/μ
η	Transformed normal coordinate
θ_b	Body angle
θ_m	Momentum thickness
θ_s	Shock angle
μ	Molecular viscosity
μ_T	Eddy viscosity
$\bar{\mu}$	Normalized molecular viscosity, μ/μ_e
ξ	Transformed surface coordinate
ρ	Density
ρ'	Fluctuating component of density
$\bar{\rho}$	Normalized density, ρ/ρ_e

LIST OF SYMBOLS (Cont)

SYMBOL	DEFINITION
σ	Reynolds number parameter, $\left[\frac{\mu^* (U_\infty^{*2} / C_p)}{\rho_\infty^* U_\infty^* a^*} \right]^{1/2}$
$\tilde{\sigma}_1, \tilde{\sigma}_2$	Parameters in turbulence model equations
Ψ_e	Stream function at boundary-layer edge
Ψ_s	Stream function at shock
<u>Superscripts</u>	
j	Zero for plane flow; 1 for axisymmetric flow
-	Quantity divided by its corresponding edge value
*	Dimensional quantity
'	Fluctuating component
<u>Subscripts</u>	
e	Boundary-layer edge
s	Shock
w	Wall
o	Stagnation value or initial value at $\xi = 0$
∞	Freestream

TRANSITIONAL BOUNDARY-LAYER SOLUTIONS
USING A MIXING-LENGTH AND A TWO-EQUATION
TURBULENCE MODEL

E. Clay Anderson* and David C. Wilcox**
DCW Industries

1. INTRODUCTION

In a previous study by Anderson and Wilcox¹, preliminary steps were taken to incorporate a two-equation turbulence model into the viscous-shock-layer analysis presented by Anderson and Moss.^{2,3} The Wilcox-Traci⁴ modified form of Saffman's⁵ turbulence model was selected for possible application. The principal advantage of this turbulence model is that conventional boundary-layer thickness parameters do not appear explicitly. However, initial attempts to apply the model in viscous-shock-layer calculations required a boundary-layer thickness definition to avoid numerical difficulties associated with the nearly discontinuous[†] behavior^{4,5} of the model equations at the edge of the predominantly viscous portion of the shock layer. For boundary-layer applications, the location of the discontinuity has been used to define the outer integration limit^{4,5} for the model and boundary-layer equations. This procedure is difficult to apply for viscous shock layer applications since gradients in the tangential velocity component fail to vanish at the edge of the predominantly viscous region.

*Consultant

**President

[†]In a strict mathematical sense, solutions to the model equations are discontinuous only in the limit of zero molecular viscosity. However, in numerical computations, solutions appear to have discontinuous derivatives because of inadequate mesh-point spacing and/or inaccurate differencing. Throughout this report, discontinuous is understood to imply solution discontinuity in the numerical sense, not in the limit of vanishing molecular viscosity.

In addition to the numerical difficulties associated with the discontinuous behavior of the model equations, it is unclear how the model-equation boundary conditions should be specified. Most previous applications of the model equations have predicted effects of freestream turbulence, and the boundary conditions generally have been different for each class of flow considered. For applications where experimental data are unavailable, it is desirable to specify a single set of model-equation boundary conditions which can be used for a wide range of flow conditions and which result in solutions showing acceptable agreement with empirical transition-point criteria.

The boundary-layer equations are considered in the present report. The model equations are modified to permit integration without specifying any boundary-layer thickness parameters, and the same model equation boundary conditions are applied in all calculations. Solutions obtained with the two-equation turbulence model are compared with experimental data and/or corresponding solutions obtained using a two-layer mixing-length turbulence model. Agreement is satisfactory for flat plate boundary layers. For blunt bodies, results indicate that further investigation is necessary.

2. ANALYSIS

In this section, the boundary-layer equations governing laminar and turbulent flow of perfect gases or mixtures of perfect gases in chemical equilibrium are presented. Mixing length and two-equation turbulence models are formulated, and the numerical solution procedure is discussed.

2.1 GOVERNING EQUATIONS

The equations of motion governing laminar and turbulent boundary-layer flows of perfect gases or of reacting mixtures of perfect gases in chemical equilibrium are presented by Anderson and Lewis.⁶ The present analysis is the same as that of Reference 6 with the two exceptions that (1) a two-equation turbulence model and (2) provisions to account for vorticity interaction effects are included. The vorticity interaction analysis is restricted to purely constant or constant effective gamma gases, but can easily be extended to mixtures of perfect gases in chemical equilibrium by including gasdynamic programs for solving the shock relations and isentropic expansions.

After non-dimensionalizing the governing equations and applying the Levy-Lees transformation to the coordinate system shown in Figure 1, the resulting equations are expressed as follows:

Continuity

$$2\xi \frac{\partial \bar{u}}{\partial \xi} + \frac{\partial V}{\partial \eta} + \bar{u} = 0 \quad (1)$$

Momentum

$$2\xi \bar{u} \frac{\partial \bar{u}}{\partial \xi} + V \frac{\partial \bar{u}}{\partial \eta} = - \frac{2\xi}{\rho_e^2 u_e^3 \mu_e} \frac{dP_e/dx}{r^2 j \bar{\rho}} - \beta \bar{u}^2 + \frac{\partial}{\partial \eta} [C(1+\epsilon^+) \frac{\partial \bar{u}}{\partial \eta}] \quad (2)$$

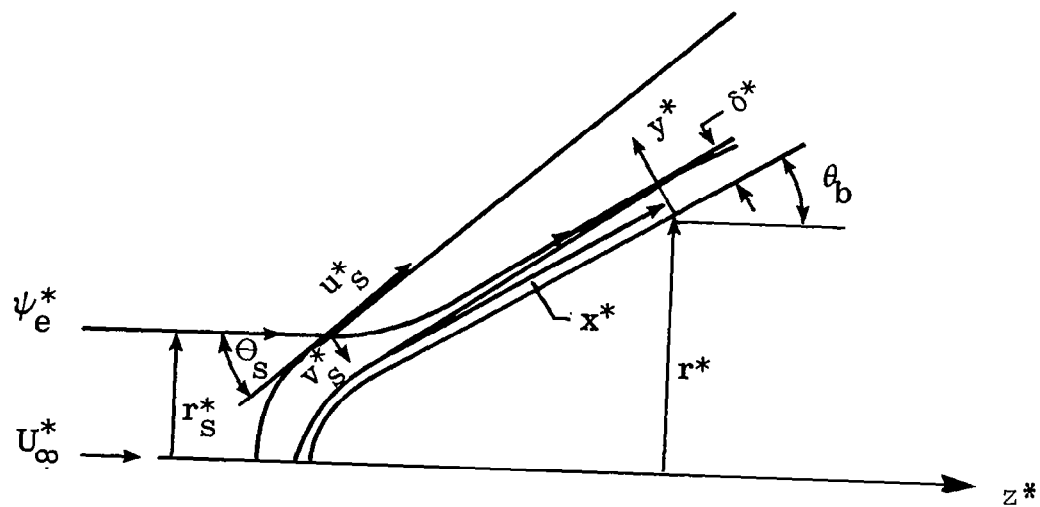


Figure 1.- Coordinate system.

Energy

$$\begin{aligned}
 2\xi \bar{u} \frac{\partial \bar{H}}{\partial \xi} + v \frac{\partial \bar{H}}{\partial \eta} &= \frac{\partial}{\partial \eta} \left[\frac{C}{N_{Pr}} \left(1 + \epsilon^+ \frac{N_{Pr}}{N_{Pr,T}} \right) \frac{\partial \bar{H}}{\partial \eta} \right] \\
 + \frac{u_e^2}{H_e} &\left\{ \left(1 - \frac{1}{N_{Pr}} \right) \left[\frac{\partial C}{\partial \eta} \bar{u} \frac{\partial \bar{u}}{\partial \eta} + C \left(\frac{\partial \bar{u}}{\partial \eta} \right)^2 + C \frac{\partial^2 \bar{u}}{\partial \eta^2} \right] \right. \\
 &\left. + C \bar{u} \frac{\partial \bar{u}}{\partial \eta} \frac{\partial}{\partial \eta} \left(1 - \frac{1}{N_{Pr}} \right) \right\}
 \end{aligned} \tag{3}$$

where

$$v = \frac{2\xi}{\rho_e \mu_e u_e r^{2j}} \left[\bar{u} \frac{\partial \eta}{\partial x} + \frac{(\rho_e \bar{\rho}_v + \bar{\rho}'_v r^j)}{(2\xi)^{1/2}} r^j \right] \tag{4}$$

$$\xi(x) = \int_0^x \rho_e u_e \mu_e r^j dx \tag{5}$$

$$\eta(x,y) = \frac{\rho_e u_e r^j}{(2\xi)^{1/2}} \int_0^y \bar{\rho} dy \tag{6}$$

$$\beta = \frac{2\xi}{\rho_e u_e^2 \mu_e r^{2j}} \frac{\partial u_e}{\partial x} \tag{7}$$

$$C = \bar{\rho} \bar{\mu} \tag{8}$$

and

$$\epsilon^+ = \mu_T / \mu \tag{9}$$

At the stagnation point,

$$V = \left[\frac{\rho_e \bar{p} v + \bar{\rho} v'}{[(j+1) \rho_e \mu_e du_e/dx]} \right]^{1/2} \quad (10)$$

$$\eta(0, y) = \left(\frac{(j+1) \rho_e du_e/dx}{\mu_e} \right)^{1/2} \int_0^y \bar{p} dy \quad (11)$$

and

$$\beta = 1/(j+1) \quad (12)$$

For laminar flows, the eddy viscosity, ϵ^+ , is set to zero. For perfect gases, the equation of state is

$$P = \frac{\gamma - 1}{\gamma} \rho T \quad (13)$$

Molecular viscosity, μ , is evaluated using Sutherland's law

$$\mu = \frac{1 + \bar{c}}{T + \bar{c}} T^{3/2}$$

where

$$\bar{c} = \frac{c^*}{(\gamma-1) M_\infty^2 T_\infty^*} \quad (14)$$

and

$$c^* = 110.3^\circ\text{K for air.}$$

Thermodynamic and transport properties for reacting gas mixtures in chemical equilibrium are functions of the composition. The procedures used to determine these properties are discussed in Reference 6.

2.1.1 Boundary Conditions for the Governing Equations

The boundary conditions at the surface, $\eta = 0$, and at the outer edge of the boundary layer, $\eta = \eta_e$, for Equations (1-3) are:

$$\begin{aligned} \bar{u} &= 0, \quad \bar{H} = \bar{H}_w, \quad v = v_w \quad \text{at } \eta = 0 \\ \bar{u} &= 1, \quad \bar{H} = 1 \quad \text{at } \eta = \eta_e \end{aligned} \tag{15}$$

The outer integration limit, η_e , is defined implicitly by the solution of Equation (2), viz:

$$v_e \left(\frac{\partial \bar{u}}{\partial \eta} \right)_e = - \frac{2\xi}{\rho_e^2 u_e^3 \mu_e r^{2j}} \frac{dP_e}{dx} - \beta - 2\xi \left(\frac{\partial \bar{u}}{\partial \xi} \right)_e \tag{16}$$

Note that unlike conventional boundary layers, $(\partial \bar{u} / \partial \eta)_e$ is non-vanishing for variable-entropy edge conditions. The solution of Equation (16) is determined by successive approximations.

2.1.2 Fluid Properties at the Boundary-Layer Edge

The method used to correct the boundary-layer edge conditions for variable entropy effects is the same as that presented by Mayne and Adams⁷. Using this method, the mass flow within the boundary layer is matched with the corresponding value at the bow shock. The shock angle is computed using the input shock geometry, and the oblique shock relations are solved. Isentropic relations are then solved to determine the corrected edge conditions (see Figure 1).

The stream-function at the local boundary-layer solution point is defined as

$$\psi_e = \rho_e u_e \int_0^{\tilde{y}_e} \frac{\tilde{y}}{\bar{\rho} \bar{u}} (r + \tilde{y} \cos \theta_b)^j d\tilde{y} \quad (17)$$

At the bow shock, the stream-function is defined as

$$\psi_s = r_s^{j+1}/j+1 \quad (18)$$

and the shock angle is

$$\theta_s = \tan^{-1}(dr_s/dz_s) \quad (19)$$

Restricting the analysis of variable-entropy effects to purely constant or constant effective γ perfect gases the oblique shock relations give:

$$P_s = \frac{1}{\gamma M_\infty^2} + \sin^2 \theta_s - v_s \sin \theta_s \quad (20)$$

$$T_s = \frac{\gamma_e - 1}{\gamma - 1} \frac{\gamma}{\gamma_e} (T_{o,\infty} - \frac{\hat{V}^2}{2}) \quad (21)$$

$$T_{o,s} = \frac{\gamma_e - 1}{\gamma - 1} \frac{\gamma}{\gamma_e} T_{o,\infty} \quad (22)$$

$$M_s = \left[\left(\frac{T_{o,s}}{T_s} - 1 \right) \frac{2}{\gamma_e - 1} \right]^{1/2} \quad (23)$$

where

$$v_s = \frac{\sin \theta_s}{\gamma_e - 1} \left\{ \frac{\gamma_e}{\gamma M_\infty^2 \sin^2 \theta_s} + \gamma_e - \left[1 + \frac{2(\gamma - \gamma_e)^2}{\gamma(\gamma - 1) M_\infty^2 \sin^2 \theta_s} + \left(\frac{\gamma_e}{\gamma M_\infty^2 \sin^2 \theta_s} \right)^2 \right]^{1/2} \right\} \quad (24)$$

$$\hat{V} = (u_s^2 + v_s^2)^{1/2} \quad (25)$$

and

$$u_s = \cos \theta_s \quad (26)$$

Isentropic expansion from the shock point to the boundary layer edge gives:

$$M_e = \left[\left(\frac{P_s}{P_e} \right)^{(\gamma_e - 1)/\gamma_e} \left(\frac{2}{\gamma_e - 1} + M_s^2 \right) - \frac{2}{\gamma_e - 1} \right]^{1/2} \quad (27)$$

$$T_e = \frac{T_{o,s}}{1 + \frac{\gamma_e - 1}{2} M_e^2} \quad (28)$$

and

$$u_e = \left[2 \left(H_e - \frac{\gamma_e - 1}{\gamma_e - 1} \frac{\gamma_e}{\gamma} T_e \right) \right]^{1/2} \quad (29)$$

The density and viscosity are determined using the equation of state and Sutherland's law.

The procedures used to define boundary-layer edge conditions at constant entropy are presented in Reference 6. Reference 6 includes the procedure for defining edge conditions for gas mixtures in chemical equilibrium. Variable entropy effects for equilibrium chemistry have not been considered.

2.2 MIXING-LENGTH TURBULENCE MODEL

The two-layer eddy-viscosity model introduced by Cebeci⁸ is used in the present report as a basis of comparison. This model assumes that the inner law formulated by Van Driest⁹ applies from the surface outward to the location where the eddy viscosity given by the inner law is equal to that of the outer law formulated and validated by Clauser¹⁰ and Klebanoff¹¹. The outer law applies for the remainder of the boundary layer.

2.2.1 Inner-Eddy-Viscosity Approximation

Prandtl's mixing-length concept is stated in transformed variables as:

$$\epsilon_1^+ = \frac{(\rho_e u_e \bar{\rho})^2 r^j \ell^2}{\sigma \mu_e \bar{\mu} (2\xi)^{1/2}} \left| \frac{\partial \bar{u}}{\partial \eta} \right| \quad (30)$$

The mixing-length, ℓ , is evaluated using Van Driest's⁹ proposal stated as:

$$\ell = k_1 y \left[1 - \exp(-y^+/A^+) \right] \quad (31)$$

where

$$y^+ = \frac{\rho_e \bar{\rho} y}{\mu_e \bar{\mu}} \left[\frac{\mu_e u_e^2 r^j \bar{\mu}_w}{\sigma (2\xi)^{1/2}} \left(\frac{\partial \bar{u}}{\partial \eta} \right)_w \right]^{1/2} \quad (32)$$

The von Karman constant, k_1 , is assumed to have a value of 0.4, and the damping factor, A^+ , is assumed to have a value of 26.

2.2.2 Outer-Eddy-Viscosity Approximation

The eddy-viscosity for the outer portion of the boundary-layer is approximated using the Clauser¹⁰-Klebanoff¹¹ expression, viz:

$$\epsilon_o^+ = \frac{k_2 \rho_e u_e \bar{\rho} \delta_k}{\sigma^2 \mu_e \bar{\mu}} \gamma_{i,\eta} \quad (33)$$

where $k_2 = 0.0168$ and δ_k is defined by

$$\delta_k = \frac{\sigma(2\xi)^{1/2}}{\rho_e u_e r^j} \int_0^{\eta_e} \frac{1-\bar{u}}{\bar{\rho}} d\eta \quad (34)$$

and

$$\gamma_{i,\eta} = [1 + 5.5(\tilde{y}/\delta)^6]^{-1} \quad (35)$$

The boundary-layer edge is assumed to be located at the point where $\bar{u} = 0.995$. Note that Equation (35) is Cebeci's⁸ approximation of the error-function definition presented by Klebanoff¹¹.

2.3 TWO-EQUATION TURBULENCE MODEL

The two-equation turbulence-model equations used in the present report are the modified form of Saffman's⁵ model presented by Wilcox and Traci⁴. In this model, the eddy viscosity is defined in terms of a turbulent mixing energy, e , and a turbulent dissipation rate, w , and is expressed as:

$$\epsilon^+ = \frac{(\rho_e \bar{\rho})^2 e}{\sigma^2 \mu_e \bar{\mu} w} \quad (36)$$

The turbulent mixing energy and turbulent dissipation rate are assumed to be governed by the following partial differential equations.

Turbulent mixing energy

$$\begin{aligned}
 2\xi\bar{u} \frac{\partial e}{\partial \xi} + v \frac{\partial e}{\partial \eta} &= \left[\alpha_1 F \left| \frac{\partial \bar{u}}{\partial \eta} \right| - \beta_1 G w \right] e \\
 &+ \frac{\partial}{\partial \eta} \left[C (1 + \tilde{\sigma}_1 \epsilon^+) \frac{\partial e}{\partial \eta} \right]
 \end{aligned} \tag{37}$$

Turbulent dissipation rate

$$\begin{aligned}
 2\xi\bar{u} \frac{\partial w^2}{\partial \xi} + v \frac{\partial w^2}{\partial \eta} &= \left\{ \alpha_2 F \left| \frac{\partial \bar{u}}{\partial \eta} \right| - \left[\beta_2 G + \frac{2\tilde{\sigma}_2 \bar{\rho}}{\sigma^2 \mu_e} \left(\frac{\partial \mathcal{X}}{\partial \eta} \right)^2 \right] w \right\} w^2 \\
 &+ \frac{\partial}{\partial \eta} \left[C (1 + \tilde{\sigma}_2 \epsilon^+) \frac{\partial w^2}{\partial \eta} \right]
 \end{aligned} \tag{38}$$

where

$$F = \frac{(2\xi)^{1/2} \bar{\rho}}{\sigma r^j \mu_e} \tag{39}$$

$$G = \frac{2\xi}{(\rho_e u_e r^j)^2 \mu_e \bar{\rho}} \tag{40}$$

and

$$\chi = \frac{\rho_e \bar{p}}{w} e^{1/2} \quad (41)$$

The six closure coefficients appearing in equations (37) and (38) have been assigned the following values by Wilcox and Traci⁴.

$$\left. \begin{aligned} \beta_1 &= \frac{9}{100} & \beta_2 &= \frac{3}{20} \\ \tilde{\sigma}_1 &= \frac{1}{2} & \tilde{\sigma}_2 &= \frac{1}{2} \\ \alpha_1 &= \frac{3}{10} \left[1 - \frac{10}{11} \exp(-2\epsilon^+) \right] \\ \alpha_2 &= \frac{1}{3} \left[1 - \frac{10}{11} \exp(-\epsilon^+/2) \right] \end{aligned} \right\} \quad (42)$$

2.3.1 Model-Equation Boundary Conditions

If the entropy at the boundary-layer edge is constant, the model equations reduce to

$$\frac{de}{d\xi} + \frac{\beta_1 w e}{(\rho_e u_e r^j)^2 \mu_e} = 0 \quad (43)$$

and

$$\frac{dw^2}{d\xi} + \frac{\beta_2 w^3}{(\rho_e u_e r^j)^2 \mu_e} = 0 \quad (44)$$

For constant fluid properties and body radius, Equations (43) and (44) can be solved analytically; the solution is:

$$e_e = \left[\frac{2(\rho_e u_e r^j)^2 \mu_e}{\beta_2 w_{e,o} \xi + 2(\rho_e u_e r^j)^2 \mu_e} \right]^{2\beta_1/\beta_2} e_{e,o} \quad (45)$$

and

$$w_e = \frac{2(\rho_e u_e r^j)^2 \mu_e}{\beta_2 w_{e,o} \xi + 2(\rho_e u_e r^j)^2 \mu_e} w_{e,o} \quad (46)$$

For more complex flows, Equations (43) and (44) are most conveniently evaluated numerically.

It is not obvious how $e_{e,o}$ and $w_{e,o}$ should be selected. Noting that Equation (36) reduces to

$$\epsilon_{e,o}^+ = \frac{\rho_e^2 e_{e,o}}{\sigma^2 \mu_e w_{e,o}} \quad (47)$$

at $\xi = 0$, there are three unknowns, two of which must be specified. The procedure used to define the model equation boundary condition is primarily empirical and consists of defining an eddy viscosity, $\epsilon_{e,o}^+$, and a turbulent mixing energy, $e_{e,o}$, which are assumed constant beyond the boundary-layer edge.

To establish a numerical value of $\epsilon_{e,o}^+$, the viscous-shock-layer analysis of Reference 2 has been used. By assigning different minimum values of ϵ_o^+ obtained from Cebeci's two-layer turbulence model, a unit value for ϵ_o^+ was found to have a negligible effect upon the solutions. The boundary-layer computer code of Reference 12 with modifications to include the two-equation turbulence model was used to define $e_{e,o}$. The value of $e_{e,o}$ selected was based upon a large number of calculations for flat-plate boundary layers. These calculations were made assuming that the momentum thickness Reynolds number at the transition point is 1000 ($\pm 15\%$) for smooth surfaces. The boundary conditions used in all calculations presented herein are:

$$\left. \begin{aligned} \rho_e e_{e,o} &= 3/2 (\tilde{T}_i/100)^2 \\ \epsilon_{e,o}^+ &= 1 \\ w_{e,o} &= \rho_e^2 e_{e,o} / (\sigma^2 \mu_e \epsilon_{e,o}^+) \end{aligned} \right\} \quad (48)$$

The surface boundary conditions for the model equations presented in Reference 4 are (see Wilcox and Traci⁴):

$$e = 0; \quad w_w = \frac{10}{3} \frac{(\rho_e u_e)^2 r^j}{\sigma (2\xi)^{1/2}} \bar{\rho}_w \left(\frac{\partial \bar{u}}{\partial \eta} \right)_w S \quad (49)$$

where S is a universal function of surface roughness and surface mass injection rate defined by the following functions.

$$S = \left(\frac{1}{S_R} + \frac{1}{S_B} \right)^{-1} \quad (50)$$

$$S_R = \left(\frac{36}{k^+} \right)^2 + \left(\frac{8}{k^+} \right)^{1/2} \quad (51)$$

$$\left. \begin{aligned} S_B &= \frac{6}{v_w^+ (1 + v_w^+)} ; \quad v_w^+ > 0 \\ S_B &= 0 ; \quad v_w^+ \leq 0 \end{aligned} \right\} \quad (52)$$

$$k^+ = \frac{\rho_e \bar{\rho}_w u_\tau k}{\sigma^2 \mu_e \bar{\mu}_w} \quad (53)$$

$$v_w^+ = \frac{v_w}{u_\tau} \quad (54)$$

and

$$u_\tau = u_e \left[\frac{\sigma \mu_e r^j \bar{\mu}_w}{(2\xi)^{1/2}} \left(\frac{\partial \bar{u}}{\partial \eta} \right)_w \right]^{1/2} \quad (55)$$

2.3.2 Modified Forms of the Model Equations

The model equations (37) and (38) with the edge conditions given in Equations (45 - 48) and with the surface boundary conditions given in Equation (49) yield solutions which exhibit rapid variations at the outer edge of the boundary layer. In numerical computations, these rapid variations generally cannot be accurately computed and the solutions appear to have discontinuous first derivatives. In References 4 and 5, these discontinuities have been used to define the outer integration limit for the boundary-layer form of the model equations. For viscous-shock-layer solutions, it is desirable to integrate the model equations from the surface to the bow shock which requires that the model equations be integrated to a distance 50 or more times the thickness of the predominantly viscous portion of the shock layer. In addition to the difficulty associated with the model equations' discontinuous behavior, the normal gradient of the tangential velocity component appearing in Equations (37) and (38) does not approach zero when vorticity interaction effects are significant for either the shock-layer or the boundary-layer equations. This and/or variable fluid properties at the edge of the boundary layer or at the bow shock for the viscous shock layer precludes reducing the model equations to analytic forms at the outer boundary. The latter difficulties have not been adequately considered in the present report, but a representative example is presented which shows the influence of vorticity interaction.

In the following paragraphs, the procedures used to eliminate the discontinuous behavior of the model equations and the modification which permits the model equations to be used for homogeneous and isotropic freestream turbulence are presented. The modified form of the model equations has been arrived at by relying upon computer optimization, some degree of empiricism, and the two-layer mixing-length turbulence model. The only restrictions imposed in

modifying the model equations are: (1) the near-wall behavior should not be significantly altered; (2) the velocity profiles, skin-friction and heat transfer distributions should show satisfactory agreement with a corresponding solution obtained using the two-layer mixing-length model and/or experimental data; and (3) the outer limit of integration for both the boundary-layer and model equations should extend several boundary-layer thicknesses outside the boundary layer.

The discontinuous behavior of the model equations near the outer edge of the boundary layer is primarily the result of the large negative gradients in the eddy viscosity. By replacing the eddy viscosity appearing in the diffusion terms of Equations (37) and (38) with the two-layer mixing-length expressions, the model equations predict an intermittent like behavior for the eddy viscosity profiles near the outer edge of the boundary layer. A number of calculations have been made to determine a formulation of the diffusion coefficient expressed in terms of model predicted variables. The suggested replacements for the diffusion terms are:

$$C(1 + \tilde{\sigma}_1 \epsilon^+) \frac{\partial e}{\partial \eta} \rightarrow C(1 + D) \frac{\partial e}{\partial \eta} \quad (56)$$

and

$$C(1 + \tilde{\sigma}_2 \epsilon^+) \frac{\partial w^2}{\partial \eta} \rightarrow C(1+D) \frac{\partial w^2}{\partial \eta} \quad (57)$$

where

$$D = \left[1 - 0.85 \exp\left(-\frac{\epsilon^+}{2}\right) \right] \epsilon^+ \quad ; \quad \frac{\partial \epsilon^+}{\partial \eta} \geq 0 \quad (58)$$

or

$$D = \left[1 - 0.85 \exp\left(-\frac{\epsilon_{\max}^+}{2}\right) \right] \epsilon_{\max}^+ \quad ; \quad \frac{\partial \epsilon^+}{\partial \eta} < 0 \quad (59)$$

If the freestream turbulence is assumed to be homogeneous and isotropic, the dissipation terms can be replaced by the following expressions:

$$\beta_1 G w \rightarrow \beta_1 G \left(\frac{w - w_e + |w - w_e|}{2} \right) \quad (60)$$

and

$$\left[\beta_2 G + \frac{2\tilde{\sigma}_2}{\sigma^2 \mu_e} \left(\frac{\partial \chi}{\partial \eta} \right)^2 \right] w \rightarrow \left[\beta_2 G + \frac{2\tilde{\sigma}_2}{\sigma^2 \mu_e} \left(\frac{\partial \chi}{\partial \eta} \right)^2 \right] \left(\frac{w - w_e + |w - w_e|}{2} \right) \quad (61)$$

For the wide range of conditions considered in making the modification in the diffusion coefficient, best overall results were obtained when the replacements given by Equations (56 - 61) are used. The computer code provides options for selecting different combinations of diffusion coefficients and dissipation terms.

2.3.3 Description of the Numerical Method and Essential Features of the Computer Code

The numerical solution procedure used in the present report is identical to that presented in Reference 6 and in the associated computer code user's manual¹². Extensive modifications and revisions have been made to this computer code to include vorticity interaction effects and the two-equation turbulence model. However, the flow logic, basic input data, and program structure are essentially unaltered. Therefore, only a brief description of the numerical method and the procedure used to control the longitudinal stepsize, Δx , is presented here.

For numerical solution, the second-order partial differential equations are linearized and expressed in a standard parabolic form

$$\frac{\partial^2 \phi}{\partial \eta^2} + \alpha_1 \frac{\partial \phi}{\partial \eta} + \alpha_2 \phi + \alpha_3 + \alpha_4 \frac{\partial \phi}{\partial \xi} = 0 \quad (63)$$

where ϕ represents \bar{u} for the momentum equation, \bar{H} for the energy equation, e for the turbulent mixing energy equation and w^2 for the turbulent dissipation rate equation. Implicit finite difference expressions are used to approximate the derivatives appearing in Equation (63). Derivatives in the normal coordinate direction are represented by three-point expressions and two-point differences are used in the longitudinal coordinate direction. When these expressions are substituted into Equation (63), the resulting difference equation is of the form:

$$A_N \phi_{M,N-1} + B_N \phi_{M,N} + C_N \phi_{M,N+1} = D_N \quad (64)$$

Equation (64), along with the boundary conditions, constitutes a system of tridiagonal form for which a number of efficient algorithms have been developed. The subscript N denotes the grid point number along the coordinate normal to the body surface, while the subscript M denotes the grid point number along the body surface.

The solution for a given body shape, freestream conditions, and pressure distribution is obtained as follows. First, the boundary-layer edge conditions are computed assuming a constant entropy expansion. At a local body station, the energy equation is solved for \bar{H} , and the momentum equation is solved to determine \bar{u} using the tridiagonal formalism. The continuity equation is then solved using the trapezoidal rule. The molecular and eddy (if turbulent) viscosities are then evaluated. When the two-equation turbulence model is used, the two model equations are integrated using the tridiagonal formalism and are iterated until the profiles for both e and w converge within specified limits. (Iteration is unnecessary if the algebraic mixing-length model is used). The eddy viscosity is then determined from the e and w distributions. The procedure is then repeated at the local body station until the governing equations and model equations simultaneously satisfy the specified convergence requirement. The solution is then marched downstream to the desired length. If vorticity interaction effects are considered, the edge conditions are recomputed and the solution is repeated.

For efficient integration of the turbulent boundary-layer equations, especially when the two-equation turbulence model is used, it is essential that the computer code include provisions for internally adjusting the longitudinal stepsize, Δx . The computer code used in the present analysis provides both external and internal control of the stepsize. In the external-control option, the stepsize is controlled by specifying a maximum permissible value of Δx , and preselecting solution points in regions where the

pressure gradients are large. In the internal-control option, Δx is controlled by monitoring the convergence rate both of the governing equations and of the model equations at the local solution station. Depending upon counters input to the program, the stepsize may be reduced either before or after the local iteration procedure is completed if the convergence rate is too slow; conversely, stepsize may be increased after the solution is obtained if the convergence rate is sufficiently fast.

For most calculations, the stepsize approaching the transition point has the maximum permissible value and is reduced by a factor of 10 or more in the transition region. Downstream of the transition region, the stepsize normally increases to the input maximum value. For the data presented in this report, the computation cost for the turbulent calculations using the two-equation model exceed that required for the two-layer mixing length model by a factor of 1.5 to 3.

3. RESULTS AND DISCUSSION

Numerical solutions of the boundary-layer equations governing laminar, transitional, and turbulent flows of perfect gases or mixtures of perfect gases in chemical equilibrium are presented in this subsection. The solutions are obtained using both the two-equation and the mixing-length turbulence model. For the two-equation model, the model-equation boundary conditions applied in all calculations are those expressed by Equations (48) with \tilde{T}_1 assigned a value of 0.13. The roughness height, k , is assumed to correspond to the smooth wall value, viz,

$$k = 100/N_{Re,\infty}$$

Unless specified, all results presented for the two-equation turbulence model have been obtained using the modifications expressed by Equations (56) thru (61).

For flat-plate boundary-layer solutions, the two-equation turbulence model results are compared with experimental data and with mixing-length turbulence model results. The transition solutions corresponding to the mixing-length model have been obtained assuming that transition is initiated at a momentum-thickness Reynolds number of 1000, and the length of the transition region is determined by assuming that the edge Reynolds number at the end of transition is two times the value at the transition point.

For blunt-body solutions, the two-equation turbulence model results are compared with corresponding solutions obtained with the mixing-length model. Transitional solutions obtained using the mixing-length model assume that transition is initiated at a momentum thickness Reynolds number of 250, and the length of the transition region is determined in the same manner as for a flat plate.

For the two-equation turbulence model, the location of the transition point and the length of the transition region are determined automatically as part of the solution to the model equations.

3.1 FLAT-PLATE BOUNDARY-LAYER CALCULATIONS

Three flat-plate boundary-layer solutions for a perfect gas and an adiabatic surface boundary condition have been obtained. These solutions correspond to the experimental data identified as Case Numbers 20, 26, and 62 in Reference 13. Figures 2, 3, and 4 show comparisons of the skin-friction distributions with experimental data for Case 20 ($M_\infty = 3.70$), Case 26 ($M_\infty = 2.58$), and Case 62 ($M_\infty = 4.54$), respectively. Numerical results corresponding to the modified form of the two-equation turbulence model and both fully developed and transitional turbulent results corresponding to the mixing-length model are presented for the three cases. For Case

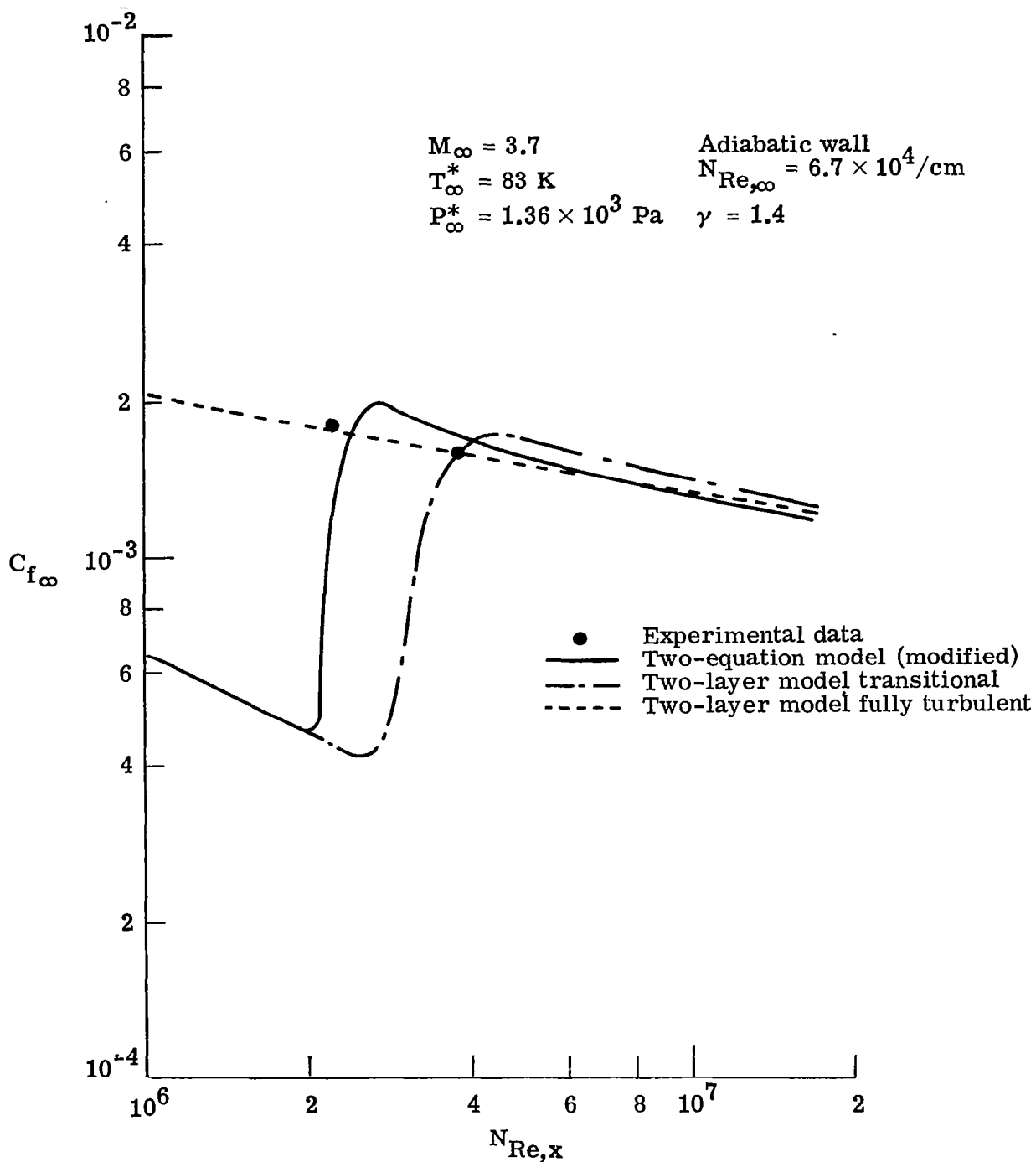


Figure 2.- Comparisons of skin-friction distributions for a flat plate - Coles Case 20.

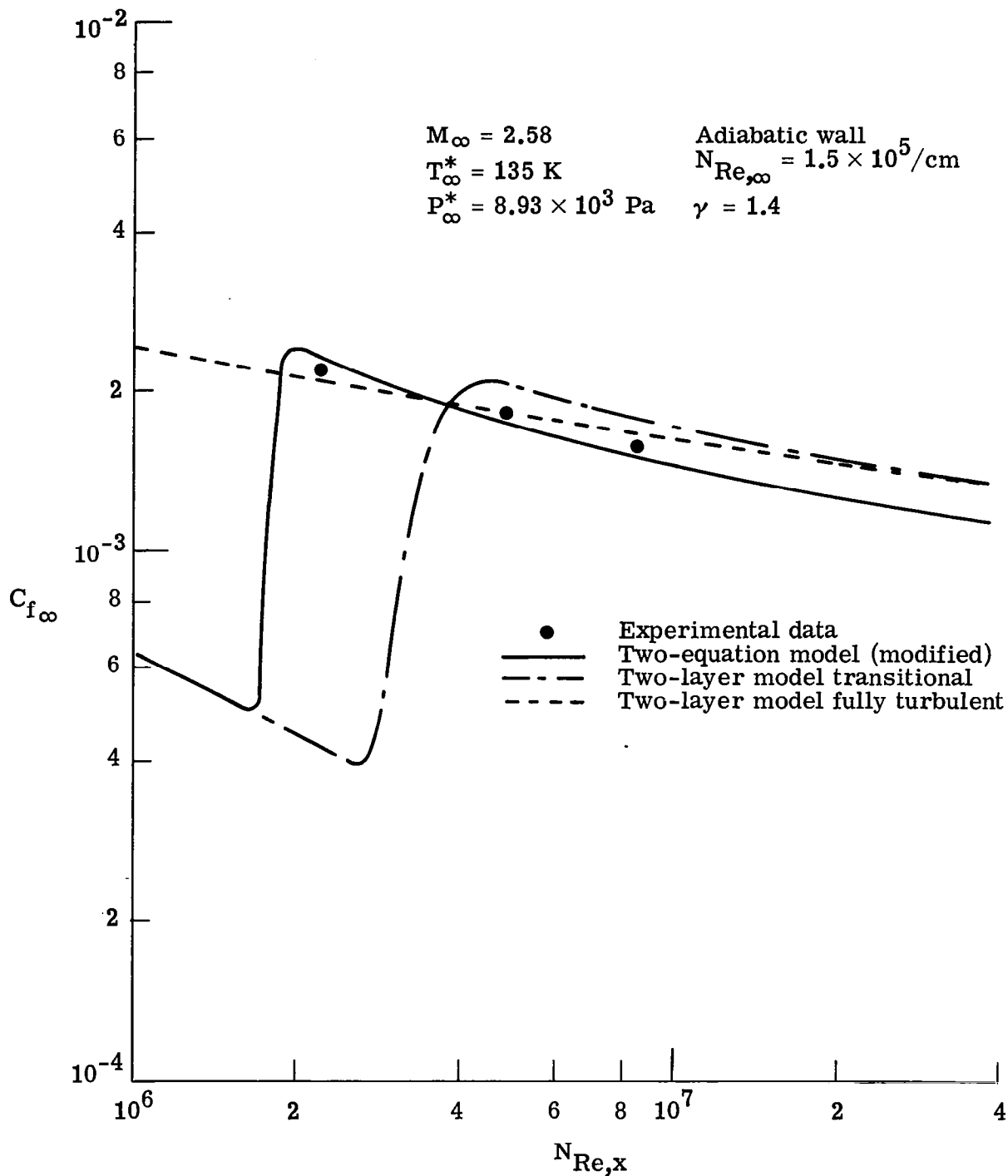


Figure 3.- Comparisons of skin-friction distributions for a flat plate - Coles Case 26.

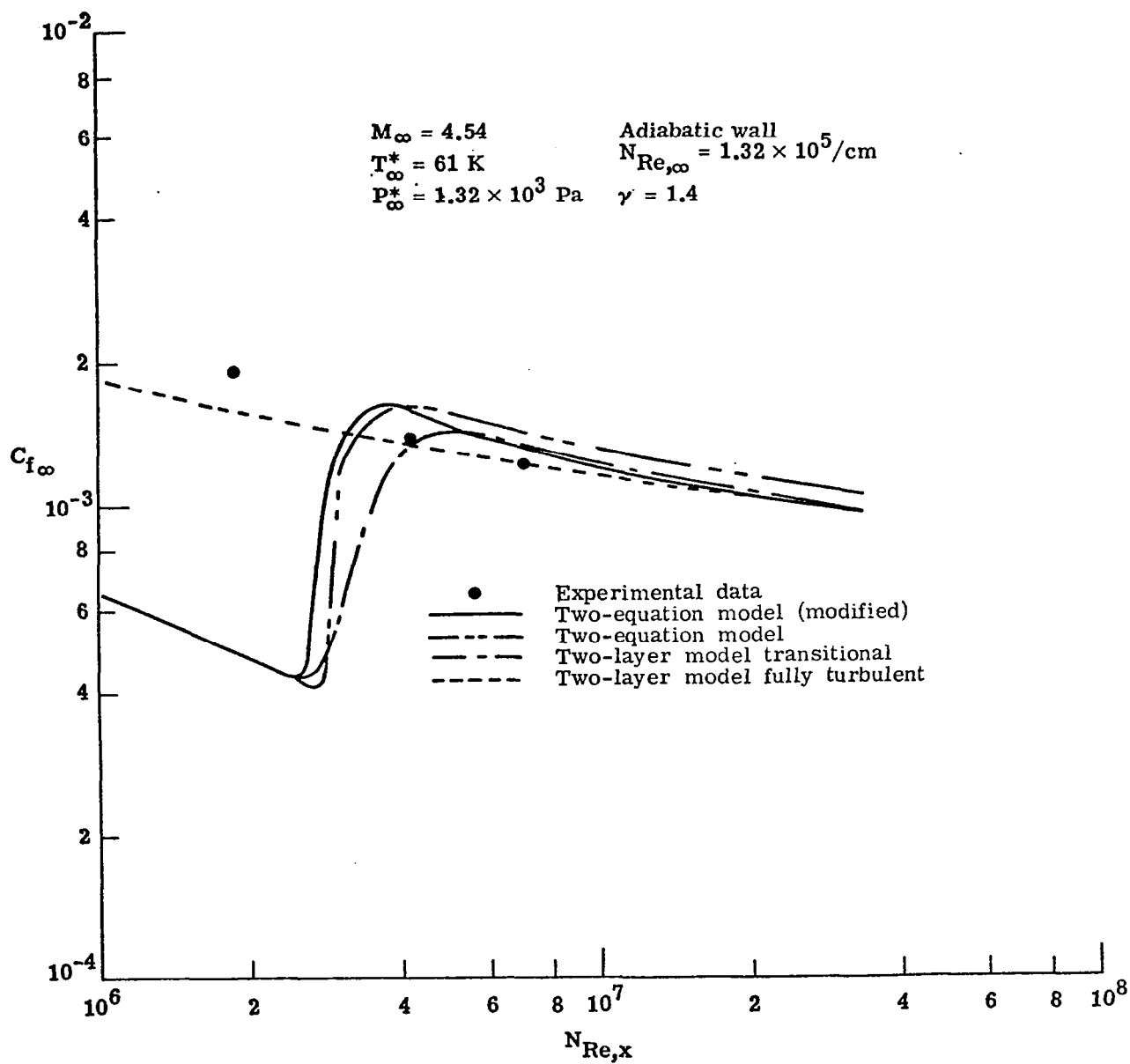


Figure 4.- Comparisons of skin-friction distributions for a flat plate - Coles Case 62.

62, the solution corresponding to the unmodified form of the two-equation model is also presented.

Results shown in Figures 2 through 4 demonstrate that fixing the model equation boundary conditions or the transition point criteria for the mixing-length model without prior knowledge of experimental data cannot result in accurate predictions of the transition point for a given problem. By treating each of the three problems separately, the experimental data can be reproduced within $\pm 3\%$ using either transitional turbulence model.

When the turbulence models are adjusted to predict the transition point at the same location, the resulting solutions show a negligible difference in the predictions for the more important boundary-layer parameters. This is illustrated by the results obtained for Case 62 where the two-equation model solution with the fixed boundary conditions and the mixing-length solution with the fixed transition point criteria predict transition at approximately the same location. For this case, comparisons of the boundary-layer thickness parameters δ , δ_c , and θ_m , and velocity profiles are presented in Figures 5 thru 8 respectively for the four solutions. The fully developed turbulent flow solution obtained with the mixing-length model is presented as a reference, and it is not expected that the transitional solutions would show general agreement with this solution. For the transitional solutions, the least satisfactory agreement is obtained for the boundary-layer thickness distributions shown in Figure 5. The modified and unmodified forms of the two-equation model predict boundary-layer thicknesses which are approximately 15% greater than that given by the transitional mixing-length model. These differences have little influence upon the boundary-layer solution and reflect minor variations in the velocity profiles near the outer edge of the boundary layer.

The comparisons of the compressible displacement thickness, δ_c , and momentum thickness, θ_m , distributions shown in Figures 6 and

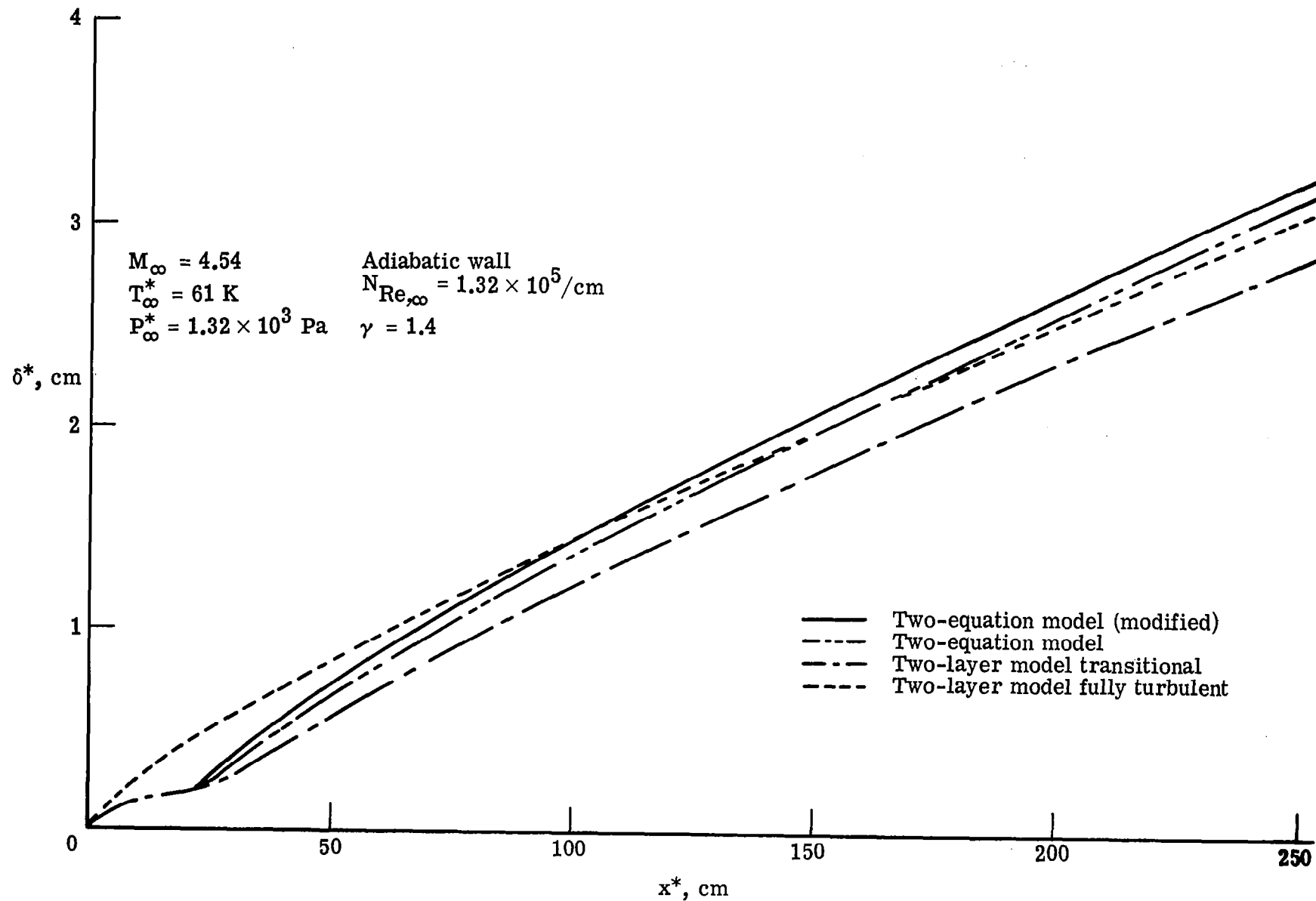


Figure 5.- Comparisons of boundary-layer thickness distributions for a flat plate - Coles Case 62.

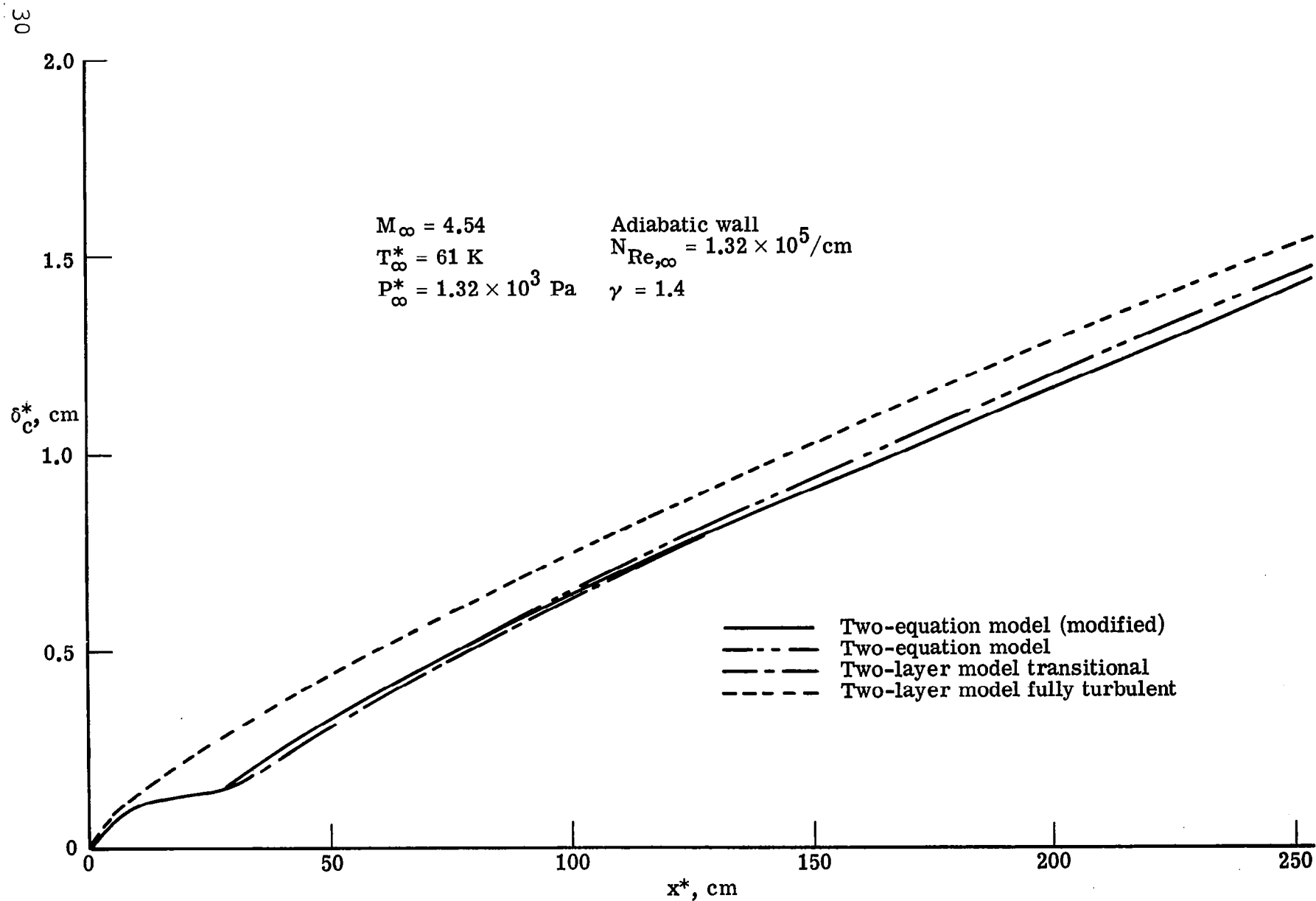


Figure 6.- Comparisons of compressible displacement thickness distributions for a flat plate - Coles Case 62.

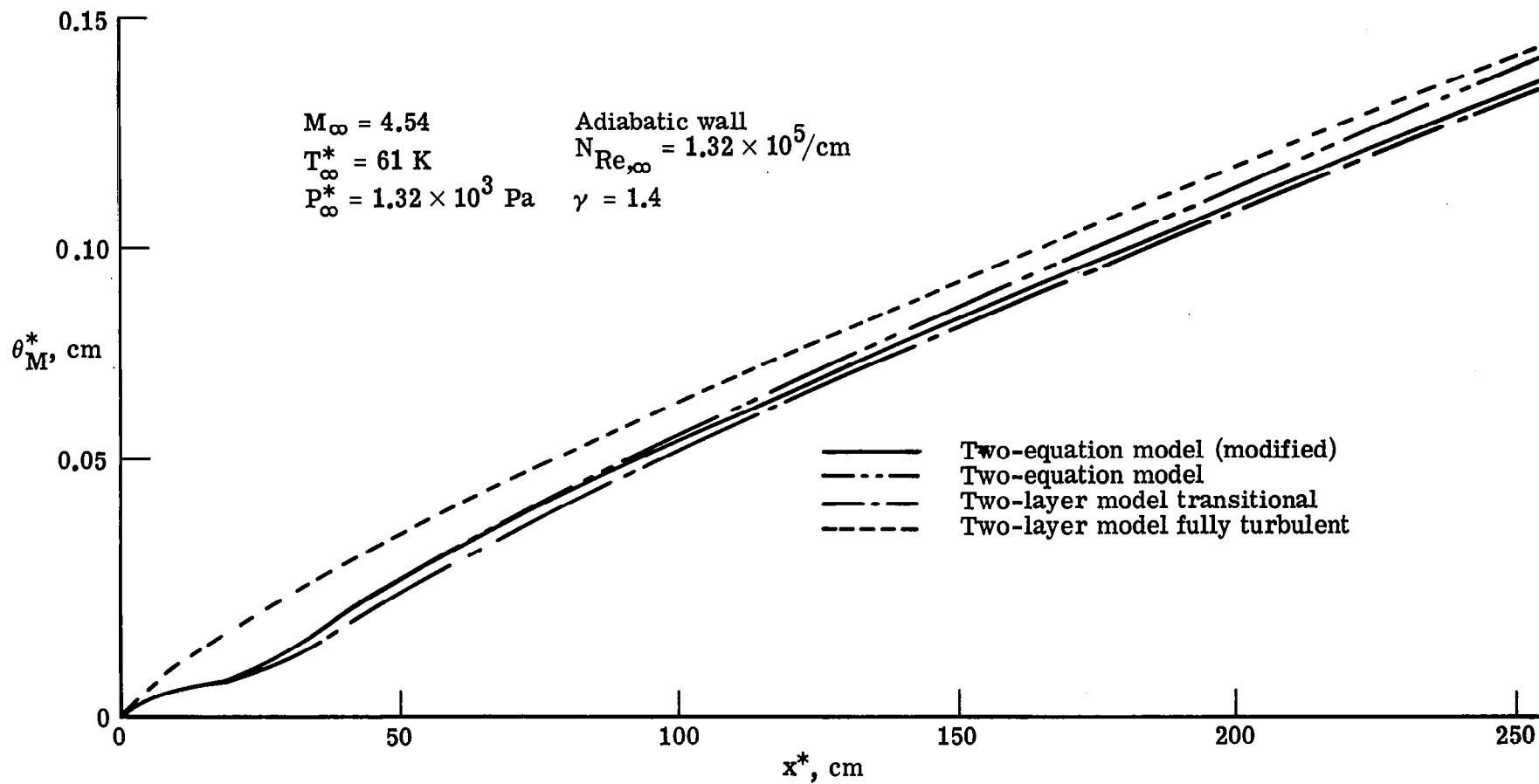


Figure 7.- Comparisons of momentum thickness distributions for a flat plate - Coles Case 62.

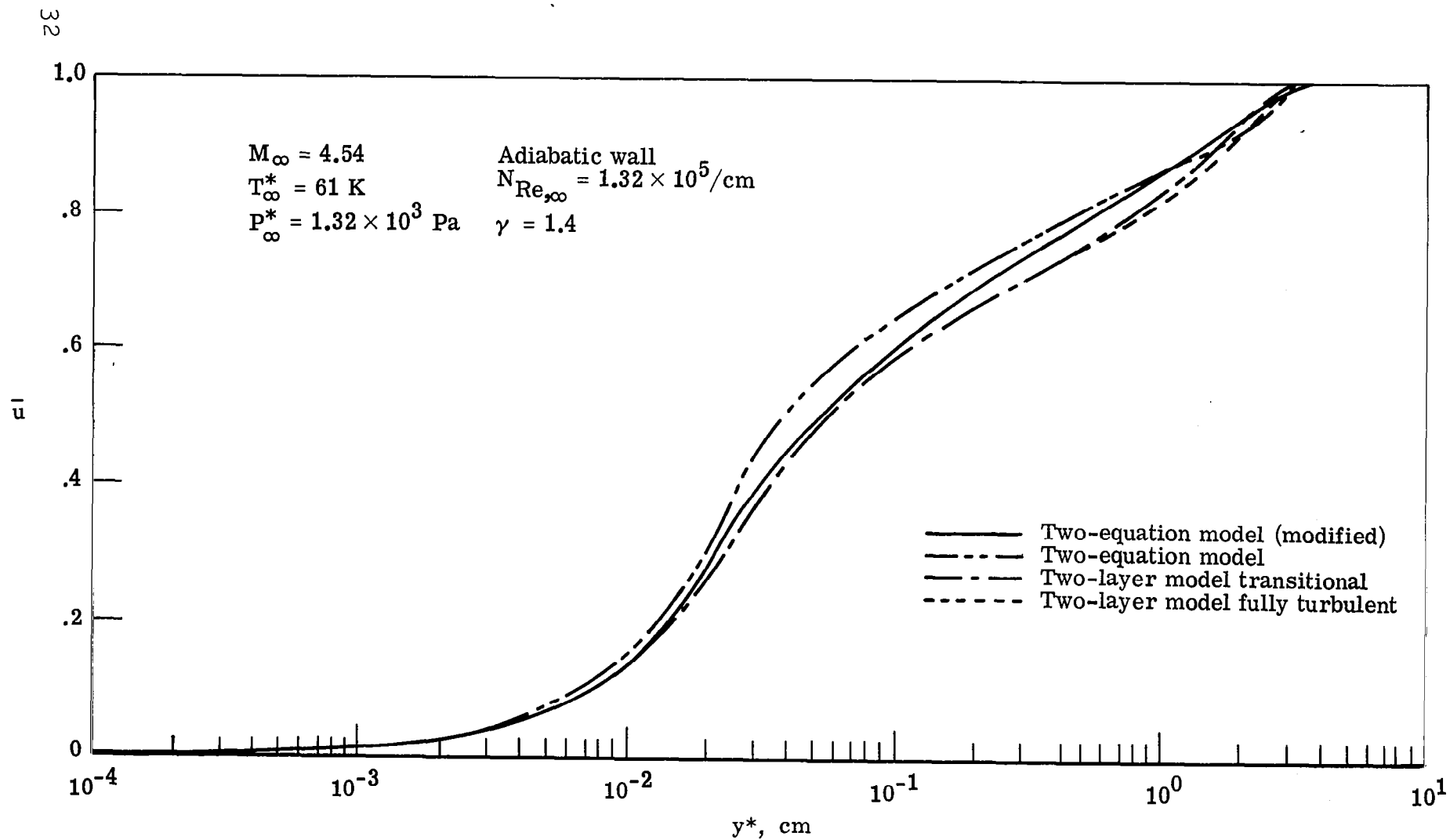


Figure 8.- Comparisons of velocity profiles at $x^* = 254 \text{ cm}$
 for a flat plate - Coles Case 62.

7, respectively, are satisfactory for the three transitional solutions.

Representative comparisons of velocity profiles for Case 62 at a location 254 cm downstream of the plate leading edge are shown in Figure 8 for the four solutions obtained. The velocity profile corresponding to the modified form of the two-equation model solution is essentially identical to the profile corresponding to the mixing-length model solution in the near-wall region and shows a maximum difference of approximately 5% through the remainder of the boundary layer. The velocity profile corresponding to the unmodified form of the two-equation turbulence model solution differs from the mixing-length solution by approximately 10% in the near-wall region and shows a maximum difference of approximately 25% through the remainder of the boundary layer. Overall agreement between the three transitional turbulence models is regarded as satisfactory.

Figure 9 shows comparisons of the Stanton number distribution obtained with the modified form of the two-equation turbulence model and the fully developed and transitional mixing-length solutions for equilibrium Mach 7.58 airflow over a flat plate. The experimental data were obtained from Reference 14. Both transitional solutions locate the transition point with sufficient accuracy for this case and show acceptable agreement with the experimental heat transfer data.

3.2 BLUNT-BODY BOUNDARY-LAYER CALCULATIONS

Solutions presented in this section corresponding to the modified form of the two-equation turbulence model represent a direct application of the modifications developed for flat-plate boundary layers to blunt-body flows. Local edge conditions for the model equations have been determined by numerical integration assuming that normal gradients of e and w vanish. Note that the replacements expressed by Equations (60) and (61) should not be used for solutions where the fluid properties at the edge of the boundary layer vary.

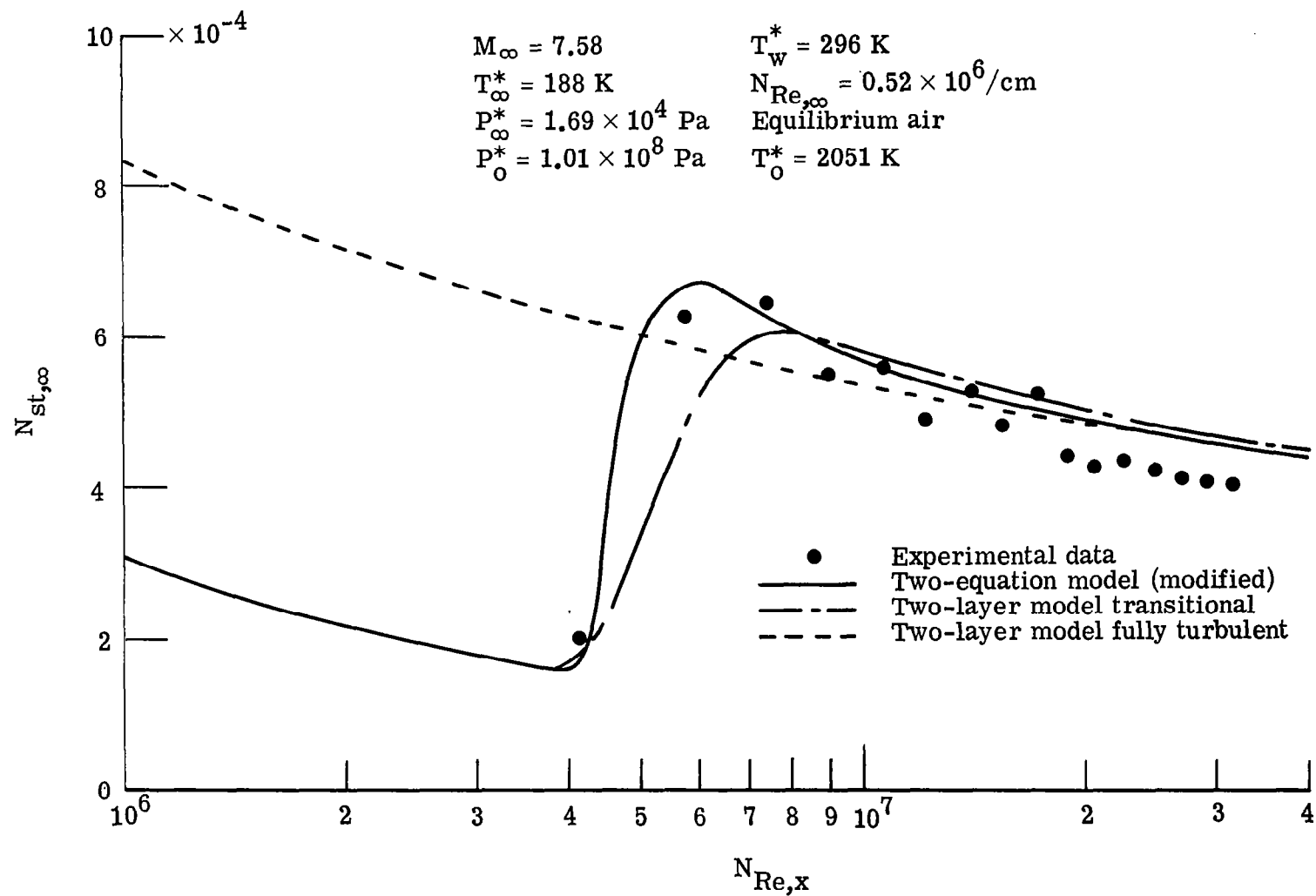


Figure 9.- Comparisons of heating-rate distributions for a flat plate - Heronimus data.

For solutions which include variable entropy effects, boundary-layer thickness, δ , is assumed to be located at the point where $\bar{H} = 0.995$ instead of $\bar{u} = 0.995$, and the outer limit of integration for the boundary-layer equations is defined by Equation (16).

The present formulation of the boundary-layer equations for solving variable entropy problems results in solutions which show excellent agreement with the viscous-shock-layer analysis of Reference 2.

Figure 10 presents heating-rate distribution along the surface of a 5 degree half-angle, spherically-blunted cone in a Mach 8 free-stream. Solutions for constant and for variable-entropy edge conditions are presented for both the modified form of the two-equation turbulence model and for the transitional mixing-length model. For the mixing-length model, the transition point was located during the first (constant entropy at the boundary-layer edge) solution pass and held fixed for subsequent solution-passes. This is consistent with the momentum-thickness Reynolds number definition for the transition point. This definition is an empirical correlation of experimental data arrived at by assuming stagnation entropy at the boundary-layer edge. In the present report, the transition point is assumed to be located at the point where the momentum thickness Reynolds number is 250 for the first solution pass. After correcting the solution for variable entropy effects, the momentum-thickness Reynolds number at the same location on the body surface is 865, and the location of the point where the momentum-thickness Reynolds number is 250 is approximately 4 cm downstream of the stagnation point instead of approximately 15 cm which was obtained for the constant entropy solution. The influence of variable entropy effects upon the laminar heating rate is not significant except at distances greater than about 16 cm downstream.

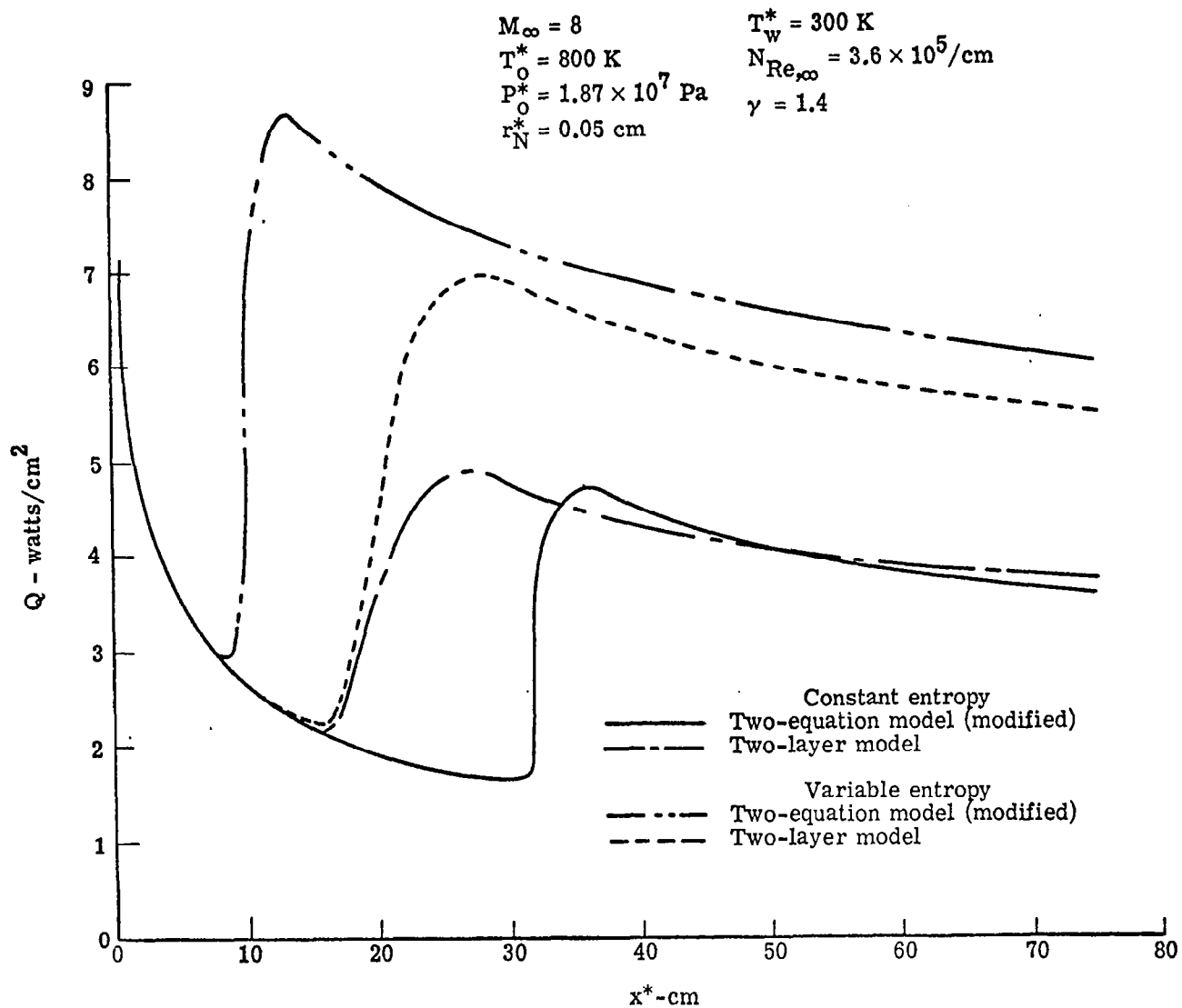


Figure 10.- Heating-rate distributions for a 5-degree half angle spherically blunted cone.

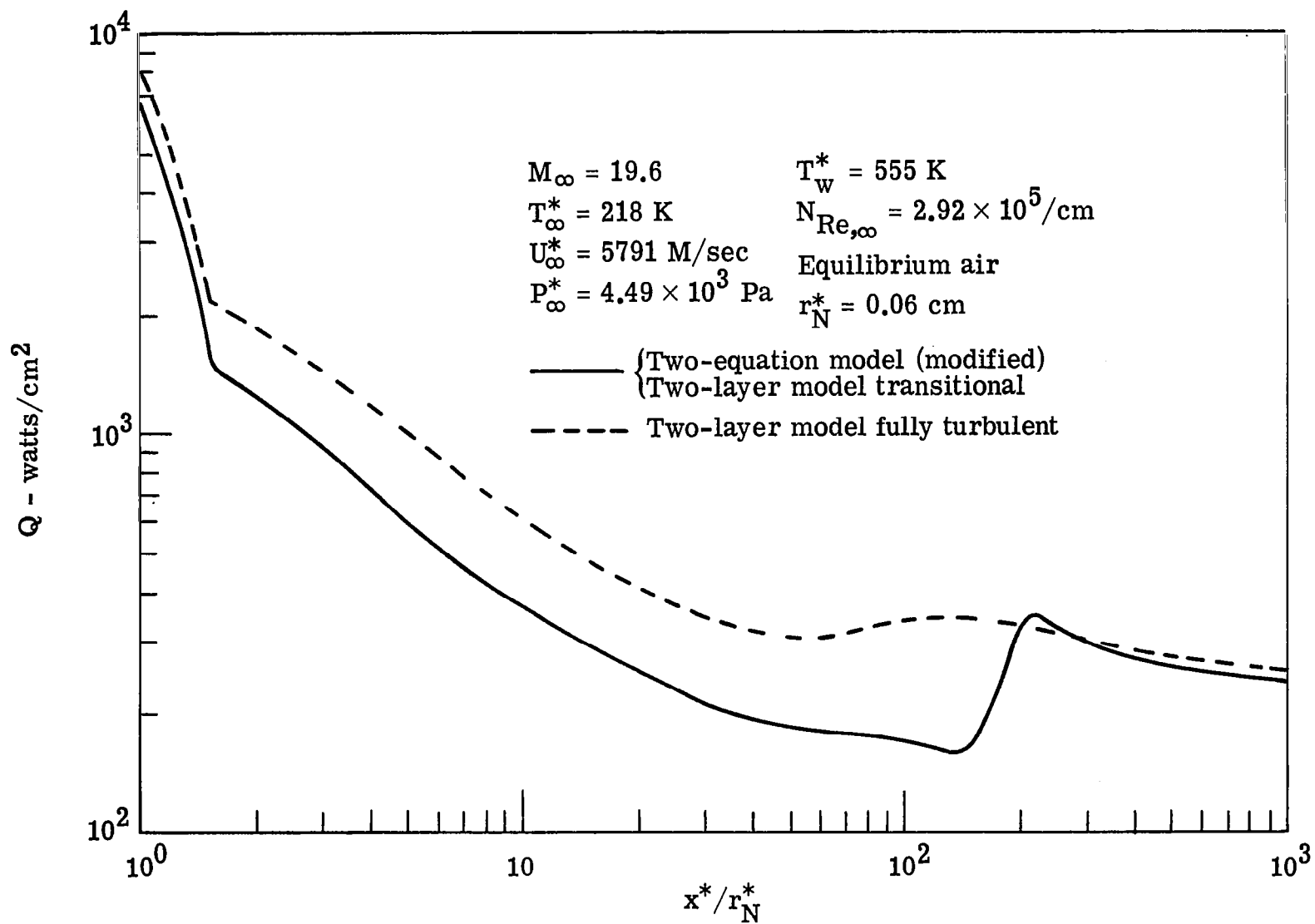


Figure 11.- Heating-rate distributions for a 5-degree half-angle spherically-blunted cone.

The two-equation turbulence model predicts transition to turbulent flow at a momentum thickness Reynolds number of approximately 400 for both the constant entropy and variable entropy edge conditions. The heating rate predictions using the two turbulence modelling techniques differ by a maximum of 5% in the fully developed turbulent region for the constant entropy edge condition solution and by approximately 10% when corrected for variable entropy edge conditions. When the two turbulence models are adjusted to predict transition at the same location on the body surface, there is no significant difference in the resulting solutions for either constant or variable entropy edge conditions.

Heating rate distributions corresponding to solutions obtained using the modified form of the two-equation turbulence model and the fully developed turbulent and transitional mixing-length model are presented in Figure 11 for a Mach 19 freestream flow over a 5-degree half-angle spherically blunted cone. This solution was obtained for an equilibrium air mixture. For this case, both transitional solutions resulted in approximately the same heating rate distribution and only the two-equation turbulence model solution is presented for the transitional case.

4. CONCLUDING REMARKS

The solutions presented for flat-plate boundary layers demonstrate that the two-equation turbulence model with a fixed set of model-equation boundary conditions provides results which show satisfactory agreement with the results obtained using the established mixing-length turbulence model and with experimental data.

For blunt bodies, the two turbulence modeling techniques result in solutions which show satisfactory agreement in the regions of fully developed turbulent flow, but the two-equation turbulence model results in large differences in the location of the transition point when corrected for variable entropy effects. The latter result is to be expected, and the adequacy of the model must be determined by further comparison with experimental data.

For the problems presented, the mixing-length turbulence model would be expected to provide adequate results and there is no specific advantage in using the more complex two-equation turbulence model. However, solutions obtained with the two-equation model do not require the definition of any boundary-layer thickness parameters which is a significant advantage when radiating flowfields or other complex flows are considered.

REFERENCES

1. Anderson, E.C., and Wilcox, D.C., "Vorticity Interaction Effects on Blunt Bodies," NASA CR-2778 (1977).
2. Anderson, E.C. and Moss, J.N., "Numerical Solution of the Viscous-Shock-Layer Equations for Hypersonic Turbulent Flow of a Perfect Gas About Blunt Axially Symmetric Bodies," NASA TN D-7865 (1975).
3. Anderson, E.C., and Moss, J.N., "Viscous-Shock-Layer Solutions for Turbulent Flow of Radiating Gas Mixtures in Chemical Equilibrium," NASA TM X-72764 (1975).
4. Wilcox, D.C., and Traci, R.M., "A Complete Model of Turbulence," AIAA Paper No 76-351, AIAA 9th Fluid and Plasma Dynamics Conference, San Diego, CA (July 1976).
5. Saffman, P.G., "A Model for Inhomogeneous Turbulent Flow," Proc Roy Soc Lon, A317, pp 417-433 (1970).
6. Anderson, E.C. and Lewis, C.H., "Laminar or Turbulent Boundary-Layer Flows of Perfect Gases or Reacting Gas Mixtures in Chemical Equilibrium," NASA CR-1893 (1971).
7. Mayne, A.W., Jr.,; and Adams, J.C., Jr., "Streamline Swallowing by Laminar Boundary Layers in Hypersonic Flow," AEDC-TR-71-32, (1971). (Available from DDC as AD 719 749).
8. Cibeci, T., "Behavior of Turbulent Flow Near A Porous Wall With Pressure Gradient." AIAA J, Vol 8, No 12, pp 2152-2156 (1970).
9. Van Driest, E.R., "On Turbulent Flow Near A Wall," Aero Sci J, Vol 23, No 11, pp 1007-1011, 1036 (1956).
10. Clauser, F.H., "The Turbulent Boundary Layer," Advances In Applied Mathematics, Academic Press, Vol VI, pp 1-51 (1956).
11. Klebanoff, P.S., "Characteristics of Turbulence in a Boundary Layer With Pressure Gradient," NACA 1247 (1955).

12. Miner, E.W., Anderson, E.C., and Lewis, C.H., "A Computer Program for Two-Dimensional and Axisymmetric Nonreacting Perfect Gas and Equilibrium Chemically Reacting Laminar, Transitional, and/or Turbulent Boundary Layer Flows," VPI-E-71-8 (1971). (Available as NASA CR-132601).
13. Coles, D., "Measurements of Turbulent Friction on a Smooth Flat Plate in Supersonic Flow," J Aero Sci, Vol 21, No 7, pp 433-448 (July 1954).
14. Hironimus, G.A., "Hypersonic Shock Tunnel Experiments on the W7 Flat Plate Model - Expansion Side Turbulent Flow and Leading Edge Transpiration Data," CAL Rept AA-1953-Y-2, (Feb 1966).

1. Report No. NASA CR-2986		2. Government Accession No.		3. Recipient's Catalog No.	
4. Title and Subtitle Transitional Boundary-Layer Solutions Using a Mixing-Length and a Two-Equation Turbulence Model				5. Report Date April 1978	
				6. Performing Organization Code	
7. Author(s) E. Clay Anderson and David C. Wilcox				8. Performing Organization Report No.	
				10. Work Unit No.	
9. Performing Organization Name and Address DCW Industries, Inc. 4367 Troost Avenue Studio City, California 91604				11. Contract or Grant No. NAS1-14517	
				13. Type of Report and Period Covered Contractor Report	
12. Sponsoring Agency Name and Address National Aeronautics and Space Administration Washington, D.C. 20546				14. Sponsoring Agency Code	
15. Supplementary Notes Technical Monitor, Kenneth Sutton, Space Systems Division, NASA Langley Research Center, Hampton, VA 23665 Topical Report					
16. Abstract Boundary-layer solutions have been obtained using the conventional two-layer mixing-length turbulence model and the Wilcox-Traci two-equation model of turbulence. Both flat-plate and blunt-body geometries have been considered. The most significant result of the study is development of approximations for the two-equation model which permit streamwise stepsize comparable to that used in mixing-length computations. Prior to this study, calculations with the two-equation model could be made only by using stepsizes an order of magnitude smaller than those used in corresponding mixing-length computations. Additionally, a set of model-equation boundary conditions have been derived which apply equally well to both flat-plate and blunt-body geometries. Solutions obtained with the two-equation turbulence model are compared with experimental data and/or corresponding solutions obtained using the mixing-length model. Agreement is satisfactory for flat-plate boundary layers. For bount bodies, results indicate that further investigation is necessary.					
17. Key Words (Suggested by Author(s)) Turbulent Boundary Layer Turbulence Models				18. Distribution Statement Unclassified - Unlimited Subject Category 34	
				Subject Category 34	
19. Security Classif. (of this report) Unclassified	20. Security Classif. (of this page) Unclassified	21. No. of Pages 49	22. Price* \$4.50		